

RevBiFPN: The Fully Reversible Bidirectional Feature Pyramid Network

Vitaliy Chiley¹ Abhay Gupta¹ Vithursan Thangarasa¹ Anshul Samar¹ Joel Hestness¹ Dennis DeCoste¹

Abstract

Bidirectional multi-scale feature fusion promotes local and global coherence and has become a de facto design principle for networks such as HRNet and EfficientDet which target spatially sensitive tasks. When paired with high resolution inputs, these networks achieve state-of-the-art results across various computer vision tasks, but training them requires substantial accelerator memory for saving large, multi-resolution activations. These memory requirements cap network size and limit progress. By recomputing activations in the backward pass, reversible networks eliminate the need to store them. Existing reversible methods, however, are not applicable to multi-scale feature fusion. This work introduces the RevSilo, the first reversible bidirectional multi-scale feature fusion module. Stacking RevSilos, we create the RevBiFPN, a fully reversible bidirectional feature pyramid network, where reversibility enables training networks 24 times larger than if activations were saved. When trained on ImageNet1k, RevBiFPN is competitive with networks such as EfficientNet designed specifically for classification. Fine tuned for segmentation and detection, RevBiFPN is also competitive with networks such as HRNet while using only a fraction of the memory. Code: <https://github.com/Cerebras/RevBiFPN>

1. Introduction

Neural Networks have elevated state-of-the-art (SOTA) results in computer vision but often have large memory requirements that complicate training and limit scalability. While low resolution intermediate representations work well for classification tasks (LeCun et al., 1998; Krizhevsky et al.,

¹Cerebras Systems, Santa Clara, California, USA. Correspondence to: Vitaliy Chiley <vitaliy@cerebras.net>, Cerebras Systems <info@cerebras.net>.

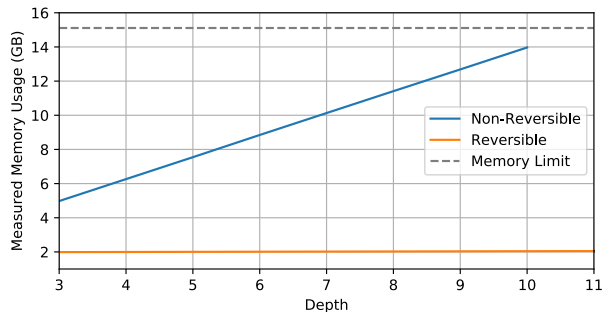


Figure 1. The measured GPU memory usage of RevBiFPN trained with and without reversible recomputation. These memory savings can be reallocated to scaling network width and input resolution.

2012; Simonyan & Zisserman, 2015; Tan & Le, 2019), dense prediction tasks, such as detection and segmentation, require the construction of high resolution feature maps which are spatially informative.

U-Net (Ronneberger et al., 2015), used for segmentation, was one of the first multi-scale feature fusion networks. While detection networks would initially process every scale of an image pyramid² independently, they soon adopted multi-scale feature fusion to directly produce feature pyramids (Lin et al., 2017a;b; Redmon & Farhadi, 2018).

Bidirectional multi-scale feature fusion networks iteratively merge information from high and low resolution feature maps producing robust models (Hendrycks & Dietterich, 2019). By iteratively aligning the semantic representations of fine grained and high level features (Figure 2), this promotes local and global coherence. As a result, these networks are often the backbone of SOTA computer vision systems, but their memory requirements complicate training and limit scalability (Liu et al., 2018; Cai & Vasconcelos, 2018; Sun et al., 2019a; Tan et al., 2020). Training these networks can push the memory bounds of modern hardware. In effect, hardware memory sets a hard limit on how far researchers scale these networks, enforcing an upper bound on network performance. Achieving SOTA frequently requires processing mega-pixel images which can consume all accelerator memory with just a single sample (Tao et al., 2020).

²often referred to as multi-scale inference

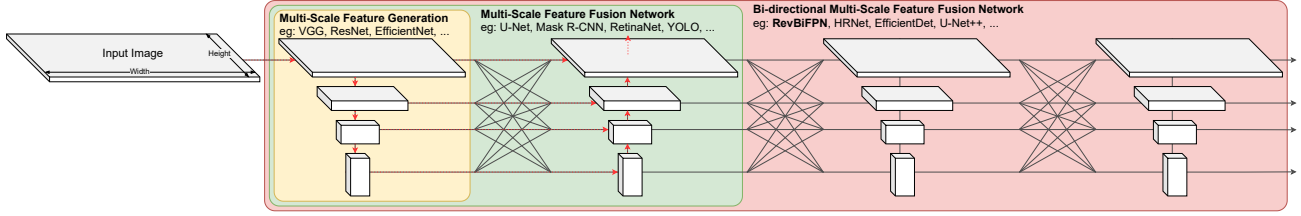


Figure 2. Connectivity of multi-scale networks. Features are depicted as boxes and the lines depict the possible connectivity of networks processing features at multiple scales. Networks like VGG (Simonyan & Zisserman, 2015), ResNet (He et al., 2016), and EfficientNet (Tan & Le, 2019) can be used to generate multi-scale features. These features are often fused by networks such as U-Net (Ronneberger et al., 2015), Mask R-CNN (He et al., 2017), or YOLO (Redmon & Farhadi, 2018) for completing spatially sensitive tasks. For example, the multi-scale connectivity of U-Net, with high resolution outputs, is identified in red. Low resolution features communicate global information, while high resolution features are able to capture detailed local information such as texture and object boundaries. By iteratively mixing high and low resolution features, bidirectional multi-scale feature fusion networks such as HRNet (Sun et al., 2019a), EfficientDet (Tan et al., 2020), and UNet++ (Zhou et al., 2018) promote local and global coherence, boosting performance in CV.

While distributed training setups can accelerate these workloads, high memory networks impose various limitations. For example, needing to use small batch sizes precludes the use of Batch Normalization (Ioffe & Szegedy, 2015), requiring batch size one alternatives (Wu & He, 2018; Chiley et al., 2019; Rao & Sohl-Dickstein, 2020; Labatie et al., 2021). Alternatively, researchers can adopt model parallel approaches to scaling models, but this often results in hardware utilization or network optimization issues (Huang et al., 2019; Chen et al., 2018a; Narayanan et al., 2019; Kosson et al., 2021).

Another approach to alleviating accelerator memory usage is to offload activations to host. However, for bandwidth constrained systems, this results in poor FLOP utilization. When performing operations with low arithmetic intensity, such as non-linearities or Depthwise Convolutions, GPUs already get poor FLOP utilization due to the limited bandwidth from device memory. Offloading activations to host memory uses even slower bandwidth, exacerbating utilization issues.

Alternatively, Griewank & Walther (2000), Dauvergne & Hascoët (2006), and Chen et al. (2016) propose gradient checkpointing³ where a subset of the intermediate activations is recomputed instead of being stored. For training neural networks of depth D , the activation memory complexity is linear with respect to the depth. Checkpointing can reduce the memory complexity from $O(D)$ to $O(\sqrt{D})$ (Chen et al., 2016). Motivated by Normalizing Flow (Dinh et al., 2017; Kingma & Dhariwal, 2018), reversible networks (Gomez et al., 2017) take this one step further. These networks are designed using a series of invertible operations which allow activation to be recomputed during the backwards pass. Using this paradigm, reversible networks perform “backpropagation without storing activations” (Gomez et al., 2017), reducing their memory complexity from linear

to constant⁴ (Figure 1). Although reversible structures have been successfully used in image classification (Gomez et al., 2017) and language modeling (Kitaev et al., 2020), they have yet to be used to produce high resolution feature maps or multi-scale feature fusion networks.

Due to the multi-scale nature of EfficientDet and HRNet, existing reversible structures cannot be directly applied as they keep tensor dimensionality constant. One approach to produce high resolution feature maps would be to apply the reversible residual block (Gomez et al., 2017) to an entire subnetwork, such as each hourglass of the Stacked Hourglass Network (Newell et al., 2016). While feasible, the entire subnetwork of activations would still need to be stored, limiting memory savings (Appendix A.1). The specific case of the hourglass design also produces high FLOP count networks (Appendix A.2) and does not provide bidirectional multi-scale feature fusion with a feature pyramid output.

1.1. Contributions

The main contributions of this work are:

1. We introduce the RevSilo (Figure 3), the first reversible bidirectional multi-scale feature fusion module.
2. We use the RevSilo to build the first fully reversible bidirectional feature pyramid network, or RevBiFPN (Figure 4), which uses a fraction of the memory used by the same network without reversibility (Figures 1 and 5).
3. With a classification head, we pretrain the network on ImageNet1k to accuracies competitive with networks

⁴When training in layer pipeline mode (Pérowski et al., 1993; Kosson et al., 2021), the complexity is quadratic with respect to depth. Reversible networks decrease the memory complexity with respect to depth from $O(D^2)$ to $O(D)$, whereas Reverse Checkpointing only decrease it to $O(D^{1.5})$ in the pipelined setting (Yang et al., 2021)).

³often referred to as reverse checkpointing

designed specifically for classification.

- Using the appropriate heads, we also show the RevBiFPN to be competitive with similar networks on detection and segmentation tasks while using a fraction of the accelerator memory for training.

2. Related Works

Deep neural networks are often used to produce low resolution features for classification tasks (LeCun et al., 1998; Krizhevsky et al., 2012; Simonyan & Zisserman, 2015; Srivastava et al., 2015; He et al., 2016; Howard et al., 2017; Tan & Le, 2019; Radosavovic et al., 2020; Ridnik et al., 2021; Dosovitskiy et al., 2021; Touvron et al., 2021; Yuan et al., 2021; Dai et al., 2021). While effective, spatially sensitive tasks, such as detection and segmentation, require the construction of high resolution feature maps. U-Net (Ronneberger et al., 2015) was among the first networks to produce high resolution feature maps. This is enabled by multi-scale feature fusion where a high to low resolution encoder is followed by a low to high resolution decoder to fuse features at multiple scales (Figure 2). The Stacked Hourglass Network (Newell et al., 2016) extends this by stacking multiple U-Net style modules to produce better quality high resolution representations. These networks are simple and serve as strong baselines in segmentation and keypoint detection.

Feature Pyramid Networks. Systems using low resolution features are often applied to image pyramids for detection (Girshick, 2015; Ren et al., 2015; Redmon et al., 2016; Redmon & Farhadi, 2017). Lin et al. (2017a) augment a pretrained classification network with a low to high resolution decoder to perform multi-scale feature fusion similar to the U-Net design. Rather than a single high resolution feature map, the network outputs features from multiple spatial resolutions to create a feature pyramid. The success of the Feature Pyramid Network (FPN) motivated similar methodologies to be used throughout the CV community (Redmon & Farhadi, 2018; Bochkovskiy et al., 2020; He et al., 2017; Lin et al., 2017b; Goyal et al., 2021). Bidirectional Feature Pyramid Networks (BiFPNs) further improve performance by iteratively applying multi-scale feature fusion modules (Tan et al., 2020; Ghiasi et al., 2019; Liu et al., 2018; Cai & Vasconcelos, 2018; Chen et al., 2018b). This allows local information from high resolution feature maps to be repeatedly fused with global information from low resolution feature maps.

FPNs are often created by using feature fusion modules to augment existing classification networks, which are not originally designed for feature fusion. However, Zhou et al. (2015), Jacobsen et al. (2017), Ke et al. (2017), Huang et al. (2018b), Sun et al. (2019a), Sun et al. (2019b), Wang et al. (2020), Cheng et al. (2020), Fan et al. (2021), and Li

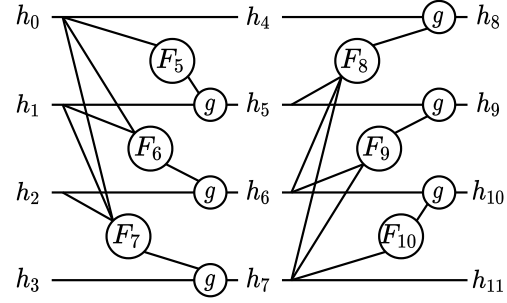


Figure 3. The Reversible Residual Silo (RevSilo). Note that the left half of the RevSilo generalizes the affine coupling block of (Dinh et al., 2014).

et al. (2021) advocate for treating bidirectional multi-scale feature fusion as a first class design principle in computer vision networks and show the effectiveness of this approach for classification, detection, and segmentation. Bidirectional multi-scale feature fusion networks reduce the semantic gap between consecutive feature maps (Zhou et al., 2018). By outputting feature pyramids, these networks allow tasks to be completed at multiple scales. This improves performance, but their memory requirements complicate training and limit scalability.

Reversible Recomputation of Activations. Reversible models (Gomez et al., 2017; Brügger et al., 2019; Pendse et al., 2020; Yamazaki et al., 2021; Sander et al., 2021; Chun et al., 2020; Kitaev et al., 2020; Nestler & Gill, 2021) save memory by recomputing activations instead of storing them. Fully reversible models have the added benefit of also being used for generation with Normalizing Flow (Dinh et al., 2014, 2017; Kingma & Dhariwal, 2018; Kingma et al., 2016; Germain et al., 2015; Papamakarios et al., 2017; Huang et al., 2018a; Jacobsen et al., 2018; Keller et al., 2021). Other approaches to reversible recomputation impose architectural limits (Bai et al., 2019), limit optimization (Behrmann et al., 2019; Thangarasa et al., 2019), or are computationally expensive (Behrmann et al., 2019). While any reversible model or method could be used for saving activation memory, none are directly applicable to bidirectional multi-scale feature fusion.

3. Reversible Residual Silo

The Reversible Residual Silo, or RevSilo, generalizes affine coupling (Dinh et al., 2014) and the reversible residual block (Gomez et al., 2017) to create an invertible module for bidirectional multi-scale feature fusion. Figure 3 shows two halves of the RevSilo with $N = 4$ spatial resolutions. The left half communicates information down the feature pyramid and the right sends information up the feature pyramid.

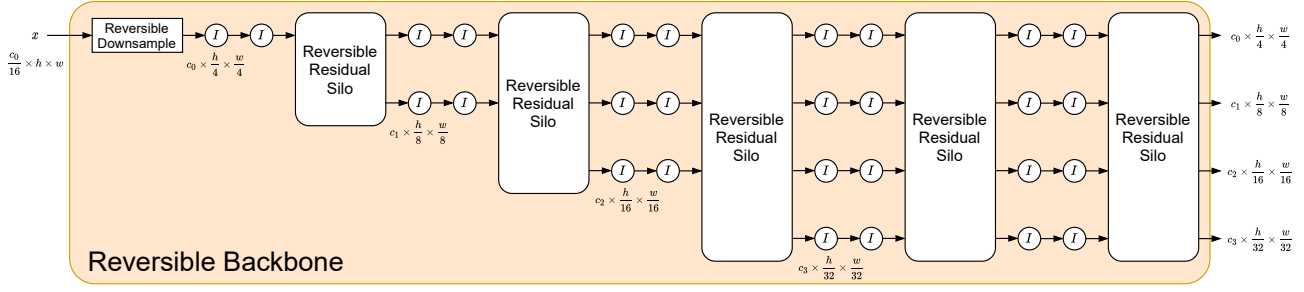


Figure 4. An RevBiFPN that creates an $N = 4$ feature pyramid where given the output feature pyramid all activations can be recomputed going backwards through the network. I are reversible residual blocks. The network uses 3 RevSilo to build the feature pyramid and has an extra depth of $d = 2$ RevSilo.

The equations for the $N = 4$ RevSilo in Figure 3 are:

$$h_4 = h_0 \quad (1)$$

$$h_5 = g(h_1, F_5(h_0)) \quad (2)$$

$$h_6 = g(h_2, F_6(h_1, h_0)) \quad (3)$$

$$h_7 = g(h_3, F_7(h_2, h_1, h_0)) \quad (4)$$

then:

$$h_8 = g(h_4, F_8(h_7, h_6, h_5)) \quad (5)$$

$$h_9 = g(h_5, F_9(h_7, h_6)) \quad (6)$$

$$h_{10} = g(h_6, F_{10}(h_7)) \quad (7)$$

$$h_{11} = h_7 \quad (8)$$

with inverse equations:

$$h_7 = h_{11} \quad (9)$$

$$h_6 = g^{-1}(h_{10}, F_{10}(h_7)) \quad (10)$$

$$h_5 = g^{-1}(h_9, F_9(h_7, h_6)) \quad (11)$$

$$h_4 = g^{-1}(h_8, F_8(h_7, h_6, h_5)) \quad (12)$$

then:

$$h_0 = h_4 \quad (13)$$

$$h_1 = g^{-1}(h_5, F_5(h_0)) \quad (14)$$

$$h_2 = g^{-1}(h_6, F_6(h_1, h_0)) \quad (15)$$

$$h_3 = g^{-1}(h_7, F_7(h_2, h_1, h_0)) \quad (16)$$

where g can be any, potentially parameterized, invertible transformation. Unless otherwise stated in this work, g is element-wise addition, and therefore its inverse, g^{-1} , is element-wise subtraction. If h_i and h_j are on the same row, i.e. $i \% N == j \% N$, the RevSilo's residual structure requires that the shape of h_i equals the shape of h_j . Otherwise, F_i should transform the shape of its inputs to match the shape of h_i . Besides this shape constraint, F_i can be any transformation. We also note that inputs can be set to 0 and such constructs are still invertible. For example, setting h_3

to 0 is equivalent to expanding an $N = 3$ feature pyramid into an $N = 4$ feature pyramid.

While the backwards recompute equations must be computed in order, the forward equations allow the N hidden tensors of the RevSilo to be computed simultaneously. This enables more parallelism in the resulting inference network. It should also be noted that if the shape of $h_i = 1$ for all i , g is the addition operator, and F_i is a dot product of its inputs with a parameter vector, then the two halves of the RevSilo form Upper and Lower Unitriangular matrices. The underlying coupling structure that makes Unitriangular matrices invertible (Thoma, 2013), makes all coupling structures (Kingma et al., 2016; Germain et al., 2015; Papamakarios et al., 2017; Huang et al., 2018a; Dinh et al., 2014; Gomez et al., 2017) invertible.

4. RevBiFPN

The fully Reversible Bidirectional multi-scale feature fusion with Feature Pyramid output Network, or RevBiFPN, uses the RevSilo to create a fully reversible backbone that utilizes bidirectional multi-scale feature fusion to produce a feature pyramid output. The high level network structure of the RevBiFPN is shown in Figure 4. The output feature pyramid can then be used as an input to different task specific heads (Section 4.3).

The networks uses the invertible SpaceToDepth stem (Ridnik et al., 2021; Shi et al., 2016; Dinh et al., 2017; Jacobsen et al., 2018) to initially downsamples the input by a factor of 4 and produce $c = 4^2 * 3 = 48$ channels. The base model use $c_0 = 48$, $c_1 = 64$, $c_2 = 80$, and $c_3 = 160$ channels in its $N = 4$ spatial resolutions. As the network size is increased, the image channels are duplicated which ensures the network is fully reversible regardless of network width. The rest of the network has a structure similar to HR-Net (Sun et al., 2019a) where transformations in the same spatial resolution use Reversible Residual Blocks (Gomez et al., 2017), denoted as I , and bidirectional multi-scale

feature fusion is done using the RevSilo.

Although F_i can be any transformation of its inputs that appropriately modifies the activation’s resolutions, for simplicity the network uses the sum of independent transformations for each input (Appendix B show the RevSilo variant used in this work.). The network isn’t designed with a specific hardware target in mind and therefore uses the MB-Conv (Howard et al., 2017) building block, a building block that efficiently utilizes parameter and multiply-accumulates (MAC) ⁵. Without a specific hardware target, we are effectively designing for MAC count used as a proxy for run time (Dehghani et al., 2021).

The RevSilo up and down samples features by factors of 2. To upsample a feature by a factor of 2^k , the Depthwise Convolution of the MBConv block uses a stride of 1 and has a kernel size of 3 or 5; this is then followed by bilinear upsampling. To downsample a feature by a factor of 2^k , the Depthwise Convolution of the MBConv block uses a stride of 2^k and has a kernel size of either $2 * 2^k - 1$ or $2 * 2^k + 1$. The MBConv blocks in the Reversible Residual Blocks use Depthwise Convolution with kernel sizes 3 or 5. As a result, the network uses a rich set of kernel sizes producing a diverse set of transforms as suggested by Tan et al. (2019). Network parameters are initialized using the Kaiming Initialization (He et al., 2015). Batch Normalization’s biases are initialized to zero and weights are initialized to one, except the last normalization’s weights are initialized to zero which promotes stability at initialization (Kingma & Dhariwal, 2018).

The network uses the MBConv variant with squeeze-excite (Tan & Le, 2019) and the hard-swish non-linearity (Howard et al., 2019). To balance the parameter and MACs used, the network has larger expansion ratios on the lower resolution streams, but uses larger squeeze-excite ratios on the large resolution streams as suggested by Ridnik et al. (2021). The resulting network, with a classification head, has a parameter and MAC profile similar to common classification networks. This network is then scaled (Section 4.2) and the results can be compared to other network families on the commonly used ImageNet (Deng et al., 2009) benchmark. Further network details and implementation can be found at <https://github.com/Cerebras/RevBiFPN>.

The RevBiFPN family of networks is pretrained on ImageNet then fine-tuned on for detection and segmentation on MSCOCO and Cityscapes using MMDetection (Chen et al., 2019) and MMSegmentation (Contributors, 2020), respectively, using task specific heads (Section 4.3).

⁵ML researcher sometimes use FLOP when they mean MAC (Dollár et al., 2021). Following common practice, we use MAC to mean multiply-accumulates since FLOP generally means floating point operation.

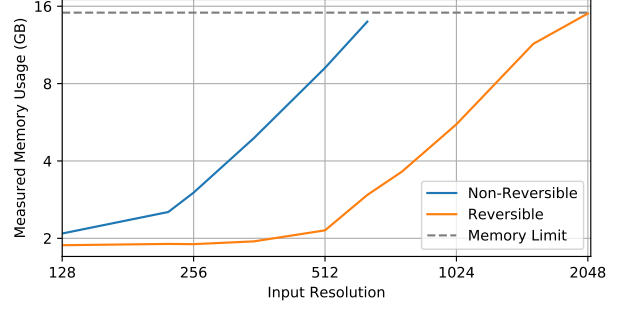


Figure 5. The measured activation memory of training a network using a batch size of 16 with and without reversible recomputation as the input resolution is scaled.

4.1. Memory Savings

The activation memory complexity of training a CV network is $O(n * c * h * w * d)$ where n is the batch size, c is the number of channels representing the network’s width, h and w are the input resolution, and d is the depth of the network. Reversible networks remove depth from the activation memory complexity of neural network training: $O(n * c * h * w)$. Naturally the question becomes: what does this practically mean? Figure 1 shows the measured memory usage of the baseline RevBiFPN network with input resolution 224×224 as the network depth is increased with and without reversibility enabled. The figure shows how the measured memory usage increases linearly when reversibility is disabled but is constant when reversibility is enabled.

A reversible and non-reversible network will have the same complexity when scaling the networks width, batch size, or input resolution, but the reversible variant will have an offset allowing much larger variants to be trained. As an example, Figure 5 shows the measured memory usage of the baseline RevBiFPN network with a batch size of 16 as the resolution is varied with and without reversibility enabled. Although scaling resolution has the same complexity for the reversible and non-reversible network, the reversible variant has an advantageous offset and can run resolutions about 4x larger than is possible with the non-reversible network. Running this experiment at a batch size of 1, on a 16GB system, the non-reversible network can process images at a resolution size of just over $2k \times 2k$ while the reversible variant can process inputs with up to a resolution of $8k \times 8k$.

4.2. Network Scaling

⁶Network size is limited by activation size, $n * c * h * w * d$, therefore activation size is used as a proxy for network size. $|\text{RevBiFPN-S6}| / |\text{RevBiFPN-S1}| = (n * 6.67c * 352 * 352 * 5) / (n * 1.33c * 256 * 256 * 2) = 23.7$

Table 1. Multiplier on width, m_w , depth, d , and input height and width of RevBiFPN trained on ImageNet at different scales. Without reversibility, the training setup would need to be modified to accommodate scales past RevBiFPN-S1. With reversibility we are able to train a network 24 times the size of its non-reversible counterpart⁶.

MODEL-SCALE	m_w	d	h AND w
RevBiFPN-S0	1	2	224
RevBiFPN-S1	1.33	2	256
RevBiFPN-S2	2	2	256
RevBiFPN-S3	2.67	3	288
RevBiFPN-S4	4	4	320
RevBiFPN-S5	5.33	4	352
RevBiFPN-S6	6.67	5	352

Once the baseline network is designed, scaling the input resolution, network width, and network depth generally results in better performance. Which dimension should be scaled and by how much? Classically, networks such as VGG (Simonyan & Zisserman, 2015) and ResNet (He et al., 2016) focused on scaling the networks depth. Tan & Le (2019) showed how compound scaling, scaling all dimensions, resulted in efficient networks at all parameter and MAC counts. In 2021, Dollár et al. showed how to scale networks such that the network run-time is minimized for large networks. Equations (4) and (5) of Dollár et al. (2021) produce a “family of scaling strategies parameterized by α ”.

In our work we use these scaling strategies setting $\alpha = 2/3$. While Dollár et al. (2021) recommend $\alpha = 4/5$, in their work Figure 6 and Figure 12 show $\alpha = 2/3$ is nearly as fast but moves some of the emphasis off width scaling to depth and resolution scaling, where Section 4.1 discusses the memory saving benefits of depth scaling in our setting. Given the outputs of the scaling rule, we choose m_w such that channel counts are multiples of 16, round the depth to an integer, and round the resolution to a multiple of 2^5 since the networks uses 5 resolution scales. Table 1 shows the different network scales used.

4.3. Network Heads

While the RevBiFPN backbone is fully reversible, it can be used with non-reversible heads. The different task heads used in the experiments are introduced here. Note that before each head is applied, a set of MBConv blocks is used as a neck, with reverse checkpointing, to transform the number of channels to 48, 64, 128, and 320 for the RevBiFPN-S0 network. The dimensionality of the neck and heads are scaled using the same width multipliers shown in Table 1. For the detection and segmentation networks the input resolution is also modified.

Classification is used to pretrain the RevBiFPN backbone before it is fine-tuned for detection and segmentation.

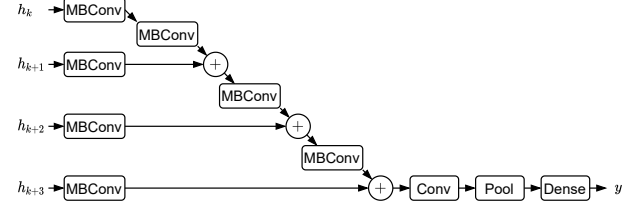


Figure 6. Neck and classification head built from a feature pyramid

The backbone outputs a feature pyramid which is transformed by the neck. The highest resolution feature map is then downsampled by a factor of 2 using an MBConv block with stride 2 and is added to the next largest feature map. This is repeated multiple times until all information is aggregated into the lowest resolution feature map. At this point a 1×1 convolution is applied, followed by global average pooling and a dense layer. The non-reversible classification head is shown in Figure 6. This design is inspired by the design in (Sun et al., 2019a) but uses the MBConv building block. When paired with a classification head, the network is denoted as RevBiFPN-C.

Segmentation is done using the XXX-XXX segmentation head provided by MMSegmentation (Contributors, 2020). When paired with a classification head, the network is denoted as RevBiFPN-S.

Detection is done with the XXX-XXX detection head provided in MMDetection (Chen et al., 2019). When paired with a classification head, the network is denoted as RevBiFPN-D.

5. Experiments

5.1. Classification

Setup The ImageNet classification task is used to pretrain the network before variants are fine tuned on downstream tasks. The different scales of the RevBiFPN-C are pre-trained for 350 epochs using 8 GPUs with a batch size of 64 per GPU. Training uses the momentum optimizer with a learning rate of 0.1, a momentum of 0.9, and an exponential moving average is used with a decay of $1 - 10^{-4}$. A 5 epoch learning rate warm-up is used with a starting learning rate of 10^{-3} . After the learning rate warm-up, a cosine decay learning rate schedule (Loshchilov & Hutter, 2017) is used with the last 10 epochs using a constant learning rate of 10^{-4} . The networks batch normalization uses a momentum of 0.9, an epsilon of 10^{-3} , and the running mean and standard deviation are averaged from all accelerators at the end of each epoch. Regularization and other training details are described in Appendix C.

Once trained, using a methodology similar to (Touvron et al., 2019; 2020), the input resolution is further optimized where

the emphasis is to produce the best performance per MAC. The input resolution of each network scale is increased and the network is fine tuned for another XX epochs at the new input resolution. The resolutions for each network are then chosen to produce best performance per MAC trade off. Previous paragraph should be modified by Anshul once he's actually done the experiments.

Results Although RevBiFPN-S0 and RevBiFPN-S1 can be trained without reversibility, Appendix D shows that reversible recomputation of activations does not hurt training. Unless otherwise stated, all of our results are shown for networks trained with reversibility. Table 2 summarizes the ImageNet classification results. While not originally designed to be to be highly competitive for classification, the RevBiFPN-C produces SOTA results when compared to classification specific networks. Talk about results when we have real results.

5.2. Segmentation

Setup fork mmsegmentation ADD STUFF Use Cityscapes or more preferably find super high resolution dataset to show off memory savings. Cityscapes uses img sizes of 1k x 2x (highly competitive: <https://paperswithcode.com/sota/semantic-segmentation-on-cityscapes>). Mapillary <https://www.mapillary.com/dataset/vistas> uses uses img sizes of 2k x 4x (+ it doesn't seem super competitive: <https://paperswithcode.com/sota/semantic-segmentation-on-mapillary-val>).

We could lean into what the HRNet/HRFormer paper do. Copy their results exactly, but use larger images to get better results....

Results ADD STUFF

5.3. Detection

Setup fork mmdetection ADD STUFF

We could lean into what the HRNet/HRFormer paper do. Copy their results exactly, but use larger images to get better results....

Results ADD STUFF

6. Conclusion

While bidirectional multi-scale feature fusion in feature pyramid networks have drastically progressed modern computer vision systems, training these networks is often limited

by accelerator memory. Reversible methods decrease the depth memory complexity of a network's activations from linear to constant, but were previously not applicable to bidirectional multi-scale feature fusion. This work introduces the RevSilo which enables the training of feature pyramid networks with bidirectional multi-scale feature fusion without the need to store network activations. The RevSilo is then used to design the RevBiFPN which is shown to be competitive for classification, segmentation, and detection with networks such as HRNet and EfficientDet all while using a fraction of the accelerator memory needed for training by its non-reversible counterparts. This makes the RevBiFPN applicable to settings which are memory constrained such as high-resolution segmentation or detection and could enable researchers to make progress on SOTA models without the needing to discard accelerators which do not have the latest memory capacity.

6.1. Future Work

Reversible networks are trained by recomputing the activations as opposed to caching them for the backwards pass. Naturally, reconstruction error, numerical precision's effect on reconstruction error, and the effect this has on optimization become potential research directions. Generally, this is a question of RevBiFPN's sensitivity to numerical precision but research could be expanded to look at RevBiFPN's sensitivity to the use of different normalizers, network sparsification methods, adversarial perturbations, and delayed gradient optimization (along with its mitigation methods (Zhang et al., 2016; Venigalla et al., 2020; Kosson et al., 2021)).

The MBConv block is still optimal when using a lightweight inference platform (Mehta & Rastegari, 2021), but exploration into the use of ResNet's BottleNeck block or Transformer's attention block could produce networks which are better optimized for GPU throughput when GPUs are the target inference hardware. Alternatively the building block could be modified to use 3D convolutional operators and the network could be applied to 3D workloads which are highly memory intensive. Future work could also explore other architectural modifications such as the use of Dilated Convolution (Yu & Koltun, 2016) or the use of weight sharing for repeated blocks in the RevBiFPN which could be used to produce more parameter efficient networks for settings where this is necessary. In general, modifying the architecture to achieve the above goals or further optimizing the current architectural design could potentially be aided by Neural Architecture Search (Tan et al., 2019; Ghiasi et al., 2019; Tan & Le, 2019). RevBiFPN generates feature pyramids at multiple semantic levels making it amenable to deep supervision which could improve performance and aid optimization (Newell et al., 2016; Zhou et al., 2018).

⁷Network is still training with 50 epochs of training left. For submission, reporting accuracy at epoch 300 but accuracy will be updated in camera ready submission.

Table 2. Models trained using only ImageNet. Where available, we also include the Top1 accuracy when using the training resolution as well as the evaluation MACs per sample at that resolution. (Probably move this Table to Appendix). While most networks are trained using 300 to 400 epochs, HRNet and RegNetY use a 100 epoch training schedule.

MODEL	PARAMS	TRAIN RES	MACS	TOP1	EVAL RES	MACS	TOP1
RevBiFPN-S0	3.42M	224	0.30B	72.84%	(?)224		
RevBiFPN-S1	5.11M	256	0.61B	75.91%	(?)256		
RevBiFPN-S2	10.6M	256	1.36B	78.97%	(?)320		
RevBiFPN-S3	19.6M	288	3.31B	81.13%	(?)384		
RevBiFPN-S4	48.7M	320	10.6B	82.87%	(?)448		
RevBiFPN-S5	82.0M	352	21.8B	83.69%	(?)512		
RevBiFPN-S6	142.3M	352	37.9B	84.2% ⁷	(?)544		
EFFICIENTNET-B0 (TAN & LE, 2019)	5.3M	224			224	0.39B	77.1%
EFFICIENTNET-B1 (TAN & LE, 2019)	7.8M	240			240	0.70B	79.1%
EFFICIENTNET-B2 (TAN & LE, 2019)	9.2M	260			260	1.0B	80.1%
EFFICIENTNET-B3 (TAN & LE, 2019)	12M	300			300	1.8B	81.6%
EFFICIENTNET-B4 (TAN & LE, 2019)	19M	380			380	4.2B	82.9%
EFFICIENTNET-B5 (TAN & LE, 2019)	30M	456			456	9.9B	83.6%
EFFICIENTNET-B6 (TAN & LE, 2019)	43M	528			528	19B	84.0%
EFFICIENTNET-B7 (TAN & LE, 2019)	66M	600			600	37B	84.3%
EFFICIENTNETV2-S (TAN & LE, 2021)	24M	128 - 300			300	8.8B	83.9%
EFFICIENTNETV2-M (TAN & LE, 2021)	55M	128 - 380			380	24B	85.1%
EFFICIENTNETV2-L (TAN & LE, 2021)	121M	128 - 380			380	53B	85.7%
NFNET-F0 (BROCK ET AL., 2021)	72.0M	192			256	12B	83.6%
NFNET-F1 (BROCK ET AL., 2021)	133M	224			320	36B	84.7%
NFNET-F2 (BROCK ET AL., 2021)	194M	256			352	63B	85.1%
NFNET-F3 (BROCK ET AL., 2021)	255M	320			416	115B	85.7%
NFNET-F4 (BROCK ET AL., 2021)	316M	384			512	215B	85.9%
NFNET-F5 (BROCK ET AL., 2021)	377M	416			544	290B	86.0%
ViT-B/16 (DOSOVITSKIY ET AL., 2021)	86.0M	384			384	55.4B	77.91%
ViT-L/16 (DOSOVITSKIY ET AL., 2021)	307M	384			384	191B	76.53%
SWIN-T (LIU ET AL., 2021)	29M	224			224	4.5B	81.3%
SWIN-S (LIU ET AL., 2021)	50M	224			224	8.7B	83.0%
SWIN-B (LIU ET AL., 2021)	88M	224	15.4B	83.5%	384	47.0B	84.5%
COATNET-0 (DAI ET AL., 2021)	25M	224	4.2B	81.6%	384	13.4B	83.9%
COATNET-1 (DAI ET AL., 2021)	42M	224	8.4B	83.3%	384	27.4B	85.1%
COATNET-2 (DAI ET AL., 2021)	75M	224	15.7B	84.1%	384	49.8B	85.7%
COATNET-2 (DAI ET AL., 2021)	75M	224	15.7B	84.1%	512	96.7B	85.9%
COATNET-3 (DAI ET AL., 2021)	168M	224	34.7B	84.5%	384	107B	85.8%
COATNET-3 (DAI ET AL., 2021)	168M	224	34.7B	84.5%	512	203B	86.0%
HRNET-W18-C (SUN ET AL., 2019A)	21.3M	224			224	3.99B	76.8%
HRNET-W30-C (SUN ET AL., 2019A)	37.7M	224			224	7.55B	78.2%
HRNET-W32-C (SUN ET AL., 2019A)	41.2M	224			224	8.31B	78.5%
HRNET-W40-C (SUN ET AL., 2019A)	57.6M	224			224	11.8B	78.9%
HRNET-W44-C (SUN ET AL., 2019A)	67.1M	224			224	13.9B	78.9%
HRNET-W48-C (SUN ET AL., 2019A)	77.5M	224			224	16.1B	79.3%
HRNET-W64-C (SUN ET AL., 2019A)	128M	224			224	26.9B	79.5%
REGNETY-200MF (RADOSAVOVIC ET AL., 2020)	3.2M	224			224	0.2B	70.4%
REGNETY-400MF (RADOSAVOVIC ET AL., 2020)	4.3M	224			224	0.4B	74.1%
REGNETY-600MF (RADOSAVOVIC ET AL., 2020)	6.1M	224			224	0.6B	75.5%
REGNETY-800MF (RADOSAVOVIC ET AL., 2020)	6.3M	224			224	0.8B	76.3%
REGNETY-1.6GF (RADOSAVOVIC ET AL., 2020)	11.2M	224			224	1.6B	78.0%
REGNETY-3.2GF (RADOSAVOVIC ET AL., 2020)	19.4M	224			224	3.2B	79.0%
REGNETY-4.0GF (RADOSAVOVIC ET AL., 2020)	20.6M	224			224	4.0B	79.4%
REGNETY-6.4GF (RADOSAVOVIC ET AL., 2020)	30.6M	224			224	6.4B	79.9%
REGNETY-8.0GF (RADOSAVOVIC ET AL., 2020)	39.2M	224			224	8.0B	79.9%
REGNETY-12GF (RADOSAVOVIC ET AL., 2020)	51.8M	224			224	12.1B	80.3%
REGNETY-16GF (RADOSAVOVIC ET AL., 2020)	83.6M	224			224	15.9B	80.4%
REGNETY-32GF (RADOSAVOVIC ET AL., 2020)	145.0M	224			224	32.3B	81.0%

A portion of this work is dedicated at looking at the RevBiFPN performance when scaling input resolution, network width, and network depth. Future work could look to improved the proposed scaling and also explore the effect of scaling N , the number of spatial resolution in the feature pyramid. The network is regularized using weight decay, label smoothing, dropout, and RandAugment. It would be prudent to hyperparameter search the coefficients of these regularization methods, as well as survey the use of methods such as stochastic depth, color jitter, mixup, random erase, and gradient clipping to improve network performance.

Lastly, the RevSilo and RevBiFPN could be applied to other domains. The RevSilo can be used as a reversible multi-modal fusion module or for fusing information from multiple input sensors. For instance, self-driving cars use multiple imaging systems. Training these systems can be highly memory intensive but building them using the RevSilo to fuse the different inputs can provide a memory efficient solution. Similarly, given the RevBiFPN is fully reversible, it can be used for flow based generation. [Awiszus et al. \(2020\)](#) focus on the need for multi-scale processing in GAN generation. They argue multi-scale systems provides local and global coherence in the spatial domain. Prior to our work, bidirectional multi-scale feature fusion wasn't possible in flow models, but now the RevSilo and RevBiFPN can provide local and global coherence in flow based generation.

Acknowledgements

Press F to pay respects.

We thank [PERSON](#), [PERSON](#), and [PERSON](#) for their help and comments that greatly improved the manuscript. We also thank Ben Wang, Ross Wightman, Lucas Nestler, Jan XMaster, Alexander Mattick, Atli Kosson, Abhinav Venigalla, Kenyon (Chuan-Yung) Tsai, Xin Wang, [PERSON](#), [PERSON](#), and [PERSON](#) for insightful discussion.

The people listed below will be moved to one of the two sentences above or the author list.

From Cerebras: Abhay Gupta, Vithursan Thangarasa, Anshul Samar, Vinay Rao (have them read it), Shreyas Saxena (have them read it), Valentina Popescu (have them read it), Natalia Vassilieva (have them read it), Joel Hestness, and Dennis DeCoste. A portion will end up on the author list.

References

- Awiszus, M., Schubert, F., and Rosenhahn, B. TOAD-GAN: Coherent Style Level Generation From a Single Example. In *Proceedings of the AAAI Conference on Artificial Intelligence and Interactive Digital Entertainment*, 2020.
- Bai, S., Kolter, J. Z., and Koltun, V. Deep Equilibrium Models. In Wallach, H., Larochelle, H., Beygelzimer, A., d'Alché-Buc, F., Fox, E., and Garnett, R. (eds.), *Advances in Neural Information Processing Systems*, volume 32. Curran Associates, Inc., 2019.
- Behrmann, J., Grathwohl, W., Chen, R. T., Duvenaud, D., and Jacobsen, J.-H. Invertible Residual Networks. In *International Conference on Machine Learning*, pp. 573–582. PMLR, 2019.
- Bochkovskiy, A., Wang, C.-Y., and Liao, H.-Y. M. YOLOv4: Optimal Speed and Accuracy of Object Detection. *arXiv preprint arXiv:2004.10934*, 2020.
- Brock, A., De, S., Smith, S. L., and Simonyan, K. High-Performance Large-Scale Image Recognition Without Normalization. *arXiv preprint arXiv:2102.06171*, 2021.
- Brügger, R., Baumgartner, C. F., and Konukoglu, E. A Partially Reversible U-Net for Memory-Efficient Volumetric Image Segmentation. In *International Conference on Medical Image Computing and Computer-Assisted Intervention*, pp. 429–437. Springer, 2019.
- Cai, Z. and Vasconcelos, N. Cascade R-CNN: Delving into High Quality Object Detection. In *Proceedings of the IEEE Conference on Computer Vision and Pattern Recognition*, pp. 6154–6162, 2018.
- Chen, C.-C., Yang, C.-L., and Cheng, H.-Y. Efficient and Robust Parallel DNN Training Through Model Parallelism on Multi-GPU Platform. *arXiv preprint arXiv:1809.02839*, 2018a.
- Chen, K., Wang, J., Pang, J., Cao, Y., Xiong, Y., Li, X., Sun, S., Feng, W., Liu, Z., Xu, J., Zhang, Z., Cheng, D., Zhu, C., Cheng, T., Zhao, Q., Li, B., Lu, X., Zhu, R., Wu, Y., Dai, J., Wang, J., Shi, J., Ouyang, W., Loy, C. C., and Lin, D. MMDetection: Open MMLab Detection Toolbox and Benchmark. *arXiv preprint arXiv:1906.07155*, 2019.
- Chen, T., Xu, B., Zhang, C., and Guestrin, C. Training Deep Nets with Sublinear Memory Cost. *arXiv preprint arXiv:1604.06174*, 2016.
- Chen, Y., Wang, Z., Peng, Y., Zhang, Z., Yu, G., and Sun, J. Cascaded Pyramid Network for Multi-Person Pose Estimation. In *Proceedings of the IEEE Conference on Computer Vision and Pattern Recognition*, pp. 7103–7112, 2018b.

- Cheng, B., Xiao, B., Wang, J., Shi, H., Huang, T. S., and Zhang, L. HigherHRNet: Scale-Aware Representation Learning for Bottom-Up Human Pose Estimation. In *Proceedings of the IEEE/CVF Conference on Computer Vision and Pattern Recognition*, pp. 5386–5395, 2020.
- Chiley, V., Sharapov, I., Kosson, A., Koster, U., Reece, R., Samaniego de la Fuente, S., Subbiah, V., and James, M. Online Normalization for Training Neural Networks. *Advances in Neural Information Processing Systems*, 32: 8433–8443, 2019.
- Chun, I. Y., Huang, Z., Lim, H., and Fessler, J. A. Momentum-Net: Fast and Convergent Iterative Neural Network for Inverse Problems. *IEEE Transactions on Pattern Analysis and Machine Intelligence*, 2020.
- Contributors, M. MMSegmentation: OpenMMLab Semantic Segmentation Toolbox and Benchmark. <https://github.com/open-mmlab/mms Segmentation>, 2020.
- Cubuk, E. D., Zoph, B., Shlens, J., and Le, Q. V. RandAugment: Practical Automated Data Augmentation with a Reduced Search Space. In *Proceedings of the IEEE/CVF Conference on Computer Vision and Pattern Recognition Workshops*, pp. 702–703, 2020.
- Dai, Z., Liu, H., Le, Q. V., and Tan, M. CoAtNet: Marrying Convolution and Attention for All Data Sizes. *arXiv preprint arXiv:2106.04803*, 2021.
- Dauvergne, B. and Hascoët, L. The Data-Flow Equations of Checkpointing in Reverse Automatic Differentiation. In *International Conference on Computational Science*, pp. 566–573. Springer, 2006.
- Dehghani, M., Arnab, A., Beyer, L., Vaswani, A., and Tay, Y. The Efficiency Misnomer. *arXiv preprint arXiv:2110.12894*, 2021.
- Deng, J., Dong, W., Socher, R., Li, L.-J., Li, K., and Fei-Fei, L. ImageNet: A Large-Scale Hierarchical Image Database. In *2009 IEEE Conference on Computer Vision and Pattern Recognition*, pp. 248–255. IEEE, 2009.
- Dinh, L., Krueger, D., and Bengio, Y. NICE: Non-Linear Independent Components Estimation. In *International Conference on Learning Representations Workshop*, 2014.
- Dinh, L., Sohl-Dickstein, J., and Bengio, S. Density Estimation using Real NVP. In *International Conference on Learning Representations*, 2017.
- Dollár, P., Singh, M., and Girshick, R. Fast and Accurate Model Scaling. In *Proceedings of the IEEE/CVF Conference on Computer Vision and Pattern Recognition*, pp. 924–932, 2021.
- Dosovitskiy, A., Beyer, L., Kolesnikov, A., Weissenborn, D., Zhai, X., Unterthiner, T., Dehghani, M., Minderer, M., Heigold, G., Gelly, S., Uszkoreit, J., and Houlsby, N. An Image is Worth 16x16 Words: Transformers for Image Recognition at Scale. In *International Conference on Learning Representations*, 2021.
- Fan, H., Xiong, B., Mangalam, K., Li, Y., Yan, Z., Malik, J., and Feichtenhofer, C. Multiscale Vision Transformers. In *Proceedings of the IEEE/CVF International Conference on Computer Vision (ICCV)*, pp. 6824–6835, October 2021.
- Germain, M., Gregor, K., Murray, I., and Larochelle, H. Made: Masked autoencoder for distribution estimation. In *International Conference on Machine Learning*, pp. 881–889. PMLR, 2015.
- Ghiasi, G., Lin, T.-Y., and Le, Q. V. NAS-FPN: Learning Scalable Feature Pyramid Architecture for Object Detection. In *Proceedings of the IEEE/CVF Conference on Computer Vision and Pattern Recognition*, pp. 7036–7045, 2019.
- Girshick, R. Fast R-CNN. In *Proceedings of the IEEE international conference on computer vision*, pp. 1440–1448, 2015.
- Gomez, A. N., Ren, M., Urtasun, R., and Grosse, R. B. The Reversible Residual Network: Backpropagation Without Storing Activations. In *Proceedings of the 31st International Conference on Neural Information Processing Systems*, pp. 2211–2221, 2017.
- Goyal, A., Bochkovskiy, A., Deng, J., and Koltun, V. Non-deep Networks. *arXiv preprint arXiv:2110.07641*, 2021.
- Griewank, A. and Walther, A. Algorithm 799: Revolve: An Implementation of Checkpointing for the Reverse or Adjoint Mode of Computational Differentiation. *ACM Transactions on Mathematical Software (TOMS)*, 26(1): 19–45, 2000.
- He, K., Zhang, X., Ren, S., and Sun, J. Delving Deep into Rectifiers: Surpassing Human-Level Performance on ImageNet Classification. In *Proceedings of the IEEE international conference on computer vision*, pp. 1026–1034, 2015.
- He, K., Zhang, X., Ren, S., and Sun, J. Deep Residual Learning for Image Recognition. In *Proceedings of the IEEE Conference on Computer Vision and Pattern Recognition*, pp. 770–778, 2016.
- He, K., Gkioxari, G., Dollár, P., and Girshick, R. Mask R-CNN. In *Proceedings of the IEEE international conference on computer vision*, pp. 2961–2969, 2017.

- Hendrycks, D. and Dietterich, T. Benchmarking Neural Network Robustness to Common Corruptions and Perturbations. In *International Conference on Learning Representations*, 2019.
- Howard, A., Sandler, M., Chu, G., Chen, L.-C., Chen, B., Tan, M., Wang, W., Zhu, Y., Pang, R., Vasudevan, V., Le, Q. V., and Adam, H. Searching for MobileNetV3. In *Proceedings of the IEEE/CVF International Conference on Computer Vision*, pp. 1314–1324, 2019.
- Howard, A. G., Zhu, M., Chen, B., Kalenichenko, D., Wang, W., Weyand, T., Andreetto, M., and Adam, H. MobileNets: Efficient Convolutional Neural Networks for Mobile Vision Applications. *arXiv preprint arXiv:1704.04861*, 2017.
- Huang, C.-W., Krueger, D., Lacoste, A., and Courville, A. Neural Autoregressive Flows. In *International Conference on Machine Learning*, pp. 2078–2087. PMLR, 2018a.
- Huang, G., Sun, Y., Liu, Z., Sedra, D., and Weinberger, K. Q. Deep Networks with Stochastic Depth. In *European Conference on Computer Vision*, pp. 646–661. Springer, 2016.
- Huang, G., Chen, D., Li, T., Wu, F., van der Maaten, L., and Weinberger, K. Multi-Scale Dense Networks for Resource Efficient Image Classification. In *International Conference on Learning Representations*, 2018b.
- Huang, Y., Cheng, Y., Bapna, A., Firat, O., Chen, D., Chen, M., Lee, H., Ngiam, J., Le, Q. V., Wu, Y., et al. GPipe: Efficient Training of Giant Neural Networks using Pipeline Parallelism. *Advances in Neural Information Processing Systems*, 32:103–112, 2019.
- Ioffe, S. and Szegedy, C. Batch Normalization: Accelerating Deep Network Training by Reducing Internal Covariate Shift. In *International Conference on Machine Learning*, pp. 448–456. PMLR, 2015.
- Jacobsen, J.-H., Oyallon, E., Mallat, S., and Smeulders, A. W. Multiscale Hierarchical Convolutional Networks. In *International Conference on Machine Learning*. PMLR, 2017.
- Jacobsen, J.-H., Smeulders, A., and Oyallon, E. I-RevNet: Deep Invertible Networks. In *International Conference on Learning Representations*, 2018.
- Ke, T.-W., Maire, M., and Yu, S. X. Multigrid Neural Architectures. In *Proceedings of the IEEE Conference on Computer Vision and Pattern Recognition*, pp. 6665–6673, 2017.
- Keller, T. A., Peters, J. W., Jaini, P., Hoogeboom, E., Forré, P., and Welling, M. Self Normalizing Flows. In *International Conference on Machine Learning*, pp. 5378–5387. PMLR, 2021.
- Kingma, D. P. and Dhariwal, P. Glow: Generative Flow with Invertible 1x1 Convolutions. In Bengio, S., Wallach, H., Larochelle, H., Grauman, K., Cesa-Bianchi, N., and Garnett, R. (eds.), *Advances in Neural Information Processing Systems*, volume 31. Curran Associates, Inc., 2018.
- Kingma, D. P., Salimans, T., Jozefowicz, R., Chen, X., Sutskever, I., and Welling, M. Improved Variational Inference with Inverse Autoregressive FLOW. *Advances in Neural Information Processing Systems*, 29:4743–4751, 2016.
- Kitaev, N., Kaiser, Ł., and Levskaya, A. Reformer: The Efficient Transformer. In *International Conference on Learning Representations*, 2020.
- Kosson, A., Chiley, V., Venigalla, A., Hestness, J., and Koster, U. Pipelined Backpropagation at Scale: Training Large Models without Batches. *Proceedings of Machine Learning and Systems*, 3, 2021.
- Krizhevsky, A., Sutskever, I., and Hinton, G. E. ImageNet Classification with Deep Convolutional Neural Networks. *Advances in Neural Information Processing Systems*, 25: 1097–1105, 2012.
- Labatie, A., Masters, D., Eaton-Rosen, Z., and Luschi, C. Proxy-normalizing activations to match batch normalization while removing batch dependence. *arXiv preprint arXiv:2106.03743*, 2021.
- LeCun, Y. A., Bottou, L., Bengio, Y., and Haffner, P. Gradient-Based Learning Applied to Document Recognition. *Proceedings of the IEEE*, 86(11):2278–2324, 1998. doi: 10.1109/5.726791.
- Li, Y., Wu, C.-Y., Fan, H., Mangalam, K., Xiong, B., Malik, J., and Feichtenhofer, C. Improved Multiscale Vision Transformers for Classification and Detection. *arXiv preprint arXiv:2112.01526*, 2021.
- Lin, T.-Y., Dollár, P., Girshick, R., He, K., Hariharan, B., and Belongie, S. Feature Pyramid Networks for Object Detection. In *Proceedings of the IEEE Conference on Computer Vision and Pattern Recognition*, pp. 2117–2125, 2017a.
- Lin, T.-Y., Goyal, P., Girshick, R., He, K., and Dollár, P. Focal Loss for Dense Object Detection. In *Proceedings of the IEEE international conference on computer vision*, pp. 2980–2988, 2017b.

- Liu, S., Qi, L., Qin, H., Shi, J., and Jia, J. Path Aggregation Network for Instance Segmentation. In *Proceedings of the IEEE Conference on Computer Vision and Pattern Recognition*, pp. 8759–8768, 2018.
- Liu, Z., Lin, Y., Cao, Y., Hu, H., Wei, Y., Zhang, Z., Lin, S., and Guo, B. Swin Transformer: Hierarchical Vision Transformer using Shifted Windows. *arXiv preprint arXiv:2103.14030*, 2021.
- Loshchilov, I. and Hutter, F. SGDR: Stochastic Gradient Descent with Warm Restarts. In *International Conference on Learning Representations*, 2017.
- Mehta, S. and Rastegari, M. MobileViT: Light-weight, General-purpose, and Mobile-friendly Vision Transformer. *arXiv preprint arXiv:2110.02178*, 2021.
- Narayanan, D., Harlap, A., Phanishayee, A., Seshadri, V., Devanur, N., Granger, G., Gibbons, P., and Zaharia, M. PipeDream: Generalized Pipeline Parallelism for DNN Training. In *ACM Symposium on Operating Systems Principles (SOSP 2019)*, October 2019.
- Nestler, L. and Gill, D. HomebrewNLP. <https://github.com/HomebrewNLP/HomebrewNLP>, 2021.
- Newell, A., Yang, K., and Deng, J. Stacked Hourglass Networks for Human Pose Estimation. In *European Conference on Computer Vision*, pp. 483–499. Springer, 2016.
- Papamakarios, G., Pavlakou, T., and Murray, I. Masked Autoregressive Flow for Density Estimation. In Guyon, I., Luxburg, U. V., Bengio, S., Wallach, H., Fergus, R., Vishwanathan, S., and Garnett, R. (eds.), *Advances in Neural Information Processing Systems*, volume 30. Curran Associates, Inc., 2017.
- Pendse, M., Thangarasa, V., Chiley, V., Holmdahl, R., Hestness, J., and DeCoste, D. Memory Efficient 3D U-Net with Reversible Mobile Inverted Bottlenecks for Brain Tumor Segmentation. In *BrainLes@MICCAI*, 2020.
- Pérowski, A., Dreyfus, G., and Girault, C. Performance analysis of a pipelined backpropagation parallel algorithm. *IEEE Transactions on Neural Networks*, 4 6:970–81, 1993.
- Radosavovic, I., Kosaraju, R. P., Girshick, R., He, K., and Dollár, P. Designing Network Design Spaces. In *Proceedings of the IEEE/CVF Conference on Computer Vision and Pattern Recognition*, pp. 10428–10436, 2020.
- Rao, V. and Sohl-Dickstein, J. Is Batch Norm Unique? An Empirical Investigation and Prescription to Emulate the Best Properties of Common Normalizers without Batch Dependence. *arXiv preprint arXiv:2010.10687*, 2020.
- Redmon, J. and Farhadi, A. YOLO9000: Better, Faster, Stronger. In *Proceedings of the IEEE Conference on Computer Vision and Pattern Recognition*, pp. 7263–7271, 2017.
- Redmon, J. and Farhadi, A. YOLOv3: An Incremental Improvement. *arXiv preprint arXiv:1804.02767*, 2018.
- Redmon, J., Divvala, S., Girshick, R., and Farhadi, A. You Only Look Once: Unified, Real-Time Object Detection. In *Proceedings of the IEEE Conference on Computer Vision and Pattern Recognition*, pp. 779–788, 2016.
- Ren, S., He, K., Girshick, R., and Sun, J. Faster R-CNN: Towards Real-Time Object Detection with Region Proposal Networks. *Advances in Neural Information Processing Systems*, 28:91–99, 2015.
- Ridnik, T., Lawen, H., Noy, A., Baruch, E. B., Sharir, G., and Friedman, I. TRResNet: High Performance GPU-Dedicated Architecture. In *Proceedings of the IEEE/CVF Winter Conference on Applications of Computer Vision*, pp. 1400–1409, 2021.
- Ronneberger, O., Fischer, P., and Brox, T. U-Net: Convolutional Networks for Biomedical Image Segmentation. In *International Conference on Medical image computing and computer-assisted intervention*, pp. 234–241. Springer, 2015.
- Sander, M. E., Ablin, P., Blondel, M., and Peyre, G. Momentum Residual Neural Networks. In *Proceedings of the 38th International Conference on Machine Learning*, pp. 139:9276–9287. PMLR, 2021.
- Shi, W., Caballero, J., Huszár, F., Totz, J., Aitken, A. P., Bishop, R., Rueckert, D., and Wang, Z. Real-Time Single Image and Video Super-Resolution using an Efficient Sub-Pixel Convolutional Neural Network. In *Proceedings of the IEEE Conference on Computer Vision and Pattern Recognition*, pp. 1874–1883, 2016.
- Simonyan, K. and Zisserman, A. Very Deep Convolutional Networks for Large-Scale Image Recognition. In *International Conference on Learning Representations*, 2015.
- Srivastava, N., Hinton, G., Krizhevsky, A., Sutskever, I., and Salakhutdinov, R. Dropout: A Simple Way to Prevent Neural Networks from Overfitting. *The Journal of Machine Learning Research*, 15(56):1929–1958, 2014.
- Srivastava, R. K., Greff, K., and Schmidhuber, J. Highway Networks. In *International Conference on Machine Learning Deep Learning Workshop*, 2015.
- Sun, K., Xiao, B., Liu, D., and Wang, J. Deep High-Resolution Representation Learning for Human Pose Estimation. In *Proceedings of the IEEE/CVF Conference*

- on *Computer Vision and Pattern Recognition*, pp. 5693–5703, 2019a.
- Sun, K., Zhao, Y., Jiang, B., Cheng, T., Xiao, B., Liu, D., Mu, Y., Wang, X., Liu, W., and Wang, J. High-Resolution Representations for Labeling Pixels and Regions. *arXiv preprint arXiv:1904.04514*, 2019b.
- Szegedy, C., Vanhoucke, V., Ioffe, S., Shlens, J., and Wojna, Z. Rethinking the Inception Architecture for Computer Vision. In *Proceedings of the IEEE conference on computer vision and pattern recognition*, pp. 2818–2826, 2016.
- Tan, M. and Le, Q. EfficientNet: Rethinking Model Scaling for Convolutional Neural Networks. In *International Conference on Machine Learning*, pp. 6105–6114. PMLR, 2019.
- Tan, M. and Le, Q. V. Efficientnetv2: Smaller models and faster training. *arXiv preprint arXiv:2104.00298*, 2021.
- Tan, M., Chen, B., Pang, R., Vasudevan, V., Sandler, M., Howard, A., and Le, Q. V. MnasNet: Platform-Aware Neural Architecture Search for Mobile. In *Proceedings of the IEEE/CVF Conference on Computer Vision and Pattern Recognition*, pp. 2820–2828, 2019.
- Tan, M., Pang, R., and Le, Q. V. EfficientDet: Scalable and Efficient Object Detection. In *Proceedings of the IEEE/CVF Conference on Computer Vision and Pattern Recognition*, pp. 10781–10790, 2020.
- Tao, A., Sapra, K., and Catanzaro, B. Hierarchical Multi-Scale Attention for Semantic Segmentation. *arXiv preprint arXiv:2005.10821*, 2020.
- Thangarasa, V., Tsai, C.-Y., Taylor, G. W., and Köster, U. Reversible Fixup Networks for Memory-Efficient Training. In *NeurIPS Systems for ML (SysML) Workshop*, 2019.
- Thoma, M. Solving Equations of Lower Unitriangular Matrices. <https://martin-thoma.com/solving-equations-of-unipotent-lower-triangular-matrices/>, 2013.
- Touvron, H., Vedaldi, A., Douze, M., and Jegou, H. Fixing the Train-Test Resolution Discrepancy. In Wallach, H., Larochelle, H., Beygelzimer, A., d'Alché-Buc, F., Fox, E., and Garnett, R. (eds.), *Advances in Neural Information Processing Systems*, volume 32. Curran Associates, Inc., 2019.
- Touvron, H., Vedaldi, A., Douze, M., and Jégou, H. Fixing the Train-Test Resolution Discrepancy: FixEfficientNet. *arXiv preprint arXiv:2003.08237*, 2020.
- Touvron, H., Cord, M., Douze, M., Massa, F., Sablayrolles, A., and Jégou, H. Training Data-Efficient Image Transformers & Distillation Through Attention. In *International Conference on Machine Learning*, pp. 10347–10357. PMLR, 2021.
- Venigalla, A., Kosson, A., Chiley, V., and Köster, U. Adaptive Braking for Mitigating Gradient Delay. In *International Conference on Machine Learning Deep Learning Workshop*, 2020.
- Wang, J., Sun, K., Cheng, T., Jiang, B., Deng, C., Zhao, Y., Liu, D., Mu, Y., Tan, M., Wang, X., Liu, W., and Xiao, B. Deep High-Resolution Representation Learning for Visual Recognition. *IEEE Transactions on Pattern Analysis and Machine Intelligence*, 2020.
- Wightman, R. PyTorch Image Models. <https://github.com/rwightman/pytorch-image-models>, 2019.
- Wu, Y. and He, K. Group Normalization. In *Proceedings of the European Conference on Computer Vision (ECCV)*, pp. 3–19, 2018.
- Yamazaki, K., Rathour, V. S., and Le, T. Invertible Residual Network with Regularization for Effective Medical Image Segmentation. *arXiv preprint arXiv:2103.09042*, 2021.
- Yang, B., Zhang, J., Li, J., Ré, C., Aberger, C., and De Sa, C. PipeMare: Asynchronous Pipeline Parallel DNN Training. *Proceedings of Machine Learning and Systems*, 3, 2021.
- Yu, F. and Koltun, V. Multi-Scale Context Aggregation by Dilated Convolutions. In *International Conference on Learning Representations*, 2016.
- Yuan, L., Hou, Q., Jiang, Z., Feng, J., and Yan, S. VOLO: Vision Outlooker for Visual Recognition. *arXiv preprint arXiv:2106.13112*, 2021.
- Yun, S., Han, D., Oh, S. J., Chun, S., Choe, J., and Yoo, Y. CutMix: Regularization Strategy to Train Strong Classifiers With Localizable Features. In *Proceedings of the IEEE/CVF International Conference on Computer Vision*, pp. 6023–6032, 2019.
- Zhang, H., Cisse, M., Dauphin, Y. N., and Lopez-Paz, D. mixup: Beyond Empirical Risk Minimization. In *International Conference on Learning Representations*, 2018.
- Zhang, W., Gupta, S., Lian, X., and Liu, J. Staleness-aware async-sgd for distributed deep learning. In *Proceedings of the Twenty-Fifth International Joint Conference on Artificial Intelligence, IJCAI'16*, pp. 2350–2356. AAAI Press, 2016. ISBN 9781577357704.

Zhou, Y., Hu, X., and Zhang, B. Interlinked Convolutional Neural Networks for face parsing. In *International symposium on neural networks*, pp. 222–231. Springer, 2015.

Zhou, Z., Siddiquee, M. M. R., Tajbakhsh, N., and Liang, J. UNet++: A Nested U-Net Architecture for Medical Image Segmentation. In *Deep Learning in Medical Image analysis and Multimodal Learning for Clinical Decision Support*, pp. 3–11. Springer, 2018.

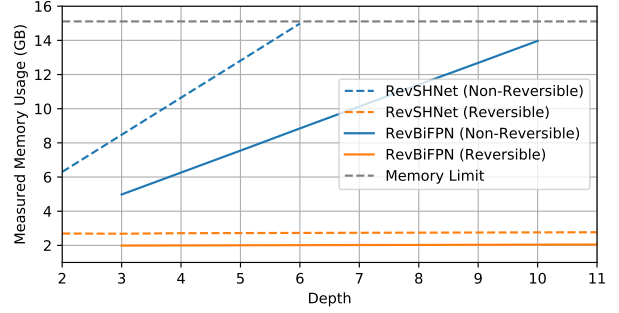


Figure 7. Memory used by RevBiFPN and RevSHNet (Non- signifies that the network has reversibility disabled) as network depth is increased.

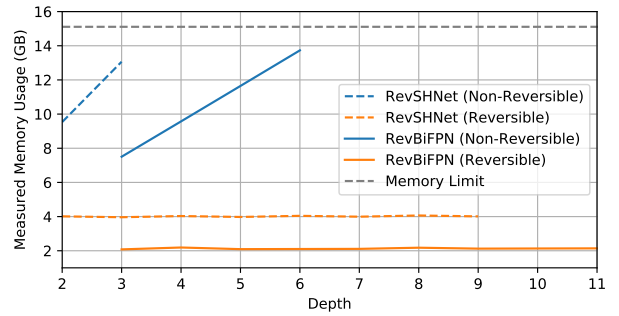


Figure 8. Reiterates the result shown in Figure 7 with an input resolution of 288 showing how RevBiFPN’s resolution scaling is preferable to scaling resolution when using the RevSHNet.

A. Stacked Hourglass Type Networks

Formerly, the reversible residual block (Gomez et al., 2017) has only been applied to networks that have constant hidden dimensionality. Stacked Hourglass (Newell et al., 2016) networks have constant hidden dimensionality and using the reversible residual block in conjunction with this network style can be used to produce high resolution feature maps in CV without the need to store hidden activations. To enable comparisons with the RevBiFPN-C we implement a Fully Reversible Stacked Hourglass Network, RevSHNet, variant using the MBConv building block, a SpaceToDepth stem, channel counts similar to the RevBiFPN channel counts, and a comparable classification head.

A.1. Memory

In the reversible setting, RevSHNet needs to store an entire hourglass of activations. With an input size of 224, this results in about a 40% increase in memory used (Figure 7). When the input size is increased to 288, RevSHNet uses almost twice the memory used by RevBiFPN (Figure 8). The increased memory usage, limits the available memory

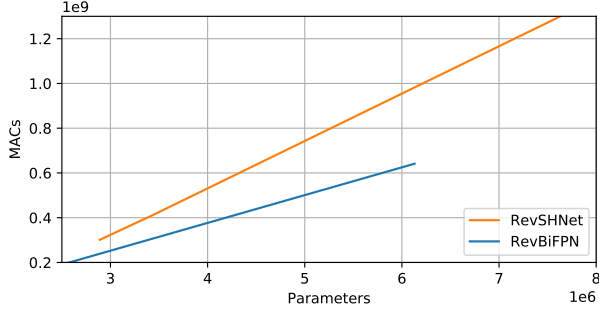


Figure 9. The MAC count of RevBiFPN and RevSHNet as network complexity (measured using parameter count) increases.

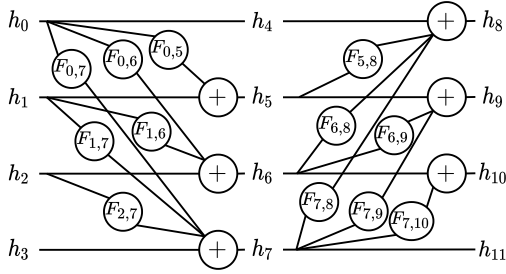


Figure 10. A RevSilo using additive coupling.

savings, ultimately limiting how much the network could be scaled.

A.2. Compute Complexity

When RevSHNet is scaled, the produced network has a high compute complexity (Figure 9) which is potentially less desirable in the long run.

The above analysis does not take into consideration network performance but we’d expect that given comparable networks, RevBiFPN would outperform RevSHNet since RevBiFPN has full bidirectional multi-scale feature fusion with a feature pyramid output where RevSHNet does not have this.

B. RevSilo with Additive Coupling

While g can be any invertible coupling function in this work we primarily use additive coupling shown in Figure 10.

C. ImageNet Training and Regularization

Training is regularized using a label smoothing (Szegedy et al., 2016) coefficient of 0.1, weight decay, dropout (Srivastava et al., 2014), stochastic depth (Huang et al., 2016), CutMix (Yun et al., 2019), mixup (Zhang et al., 2018), and the timm library (Wightman, 2019) variant of RandAug-

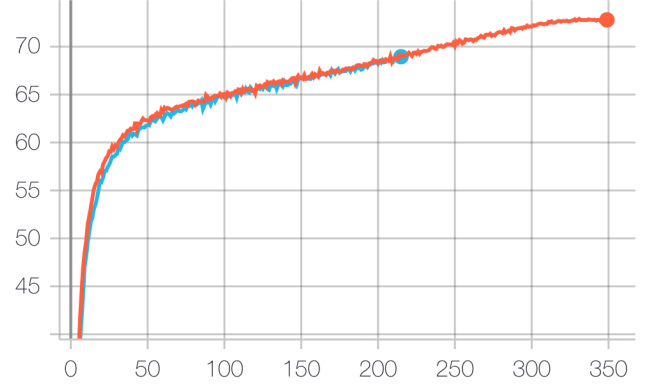


Figure 11. ImageNet training of RevBiFPN-S0 with and without reversibility (will be updated for camera-ready submission).

ment (Cubuk et al., 2020) with a magnitude of 9 and mstd set to 0.5. To prevent larger scales of the network from overfitting, regularization increases with network scale. Without knowing how much augmentation was needed for each network, training began with the regularization shown in Table 3. When the validation accuracy of the ema model began to plateau, the regularization of the models was increased. The final regularization used for each network is shown in Table 4.

D. Training With and Without Reversibility

Figure 11 shows RevBiFPN training with and without reversibility. Training with reversible recomputation of activations requires only 2GB of accelerator memory and produces results which are nearly indistinguishable from regular training which consumes 12GB of accelerator memory.

Table 3. Initial weight decay (WD), dropout, number of RandAugment ops applied (N), mixup, CutMix, and stochastic depth.

MODEL-SCALE	WD	DROPOUT	N	MIXUP	CUTMIX	STOCHASTIC DEPTH
RevBiFPN-S0	4×10^{-5}	0.25	2	0.00	0.0	0.0
RevBiFPN-S1	4×10^{-5}	0.25	2	0.00	0.0	0.0
RevBiFPN-S2	4×10^{-5}	0.25	2	0.00	0.0	0.0
RevBiFPN-S3	4×10^{-5}	0.25	2	0.00	0.0	0.0
RevBiFPN-S4	4×10^{-5}	0.4	4	0.00	0.0	0.0
RevBiFPN-S5	4×10^{-5}	0.4	4	0.00	0.0	0.0
RevBiFPN-S6	4×10^{-5}	0.5	5	0.00	0.0	0.0

Table 4. Weight decay (WD), dropout, number of RandAugment ops applied (N), mixup, CutMix, and stochastic depth used at the end of training.

MODEL-SCALE	WD	DROPOUT	N	MIXUP	CUTMIX	STOCHASTIC DEPTH
RevBiFPN-S0	4×10^{-5}	0.25	2	0.00	0.0	0.00
RevBiFPN-S1	4×10^{-5}	0.25	2	0.00	0.0	0.00
RevBiFPN-S2	4×10^{-5}	0.3	3	0.00	0.0	0.00
RevBiFPN-S3	4×10^{-5}	0.3	3	0.10	1.0	0.05
RevBiFPN-S4	2×10^{-5}	0.4	4	0.10	1.0	0.10
RevBiFPN-S5	2×10^{-5}	0.4	4	0.20	1.0	0.10
RevBiFPN-S6	2×10^{-5}	0.5	5	0.20	1.0	0.15